48th AIAA Aerospace Sciences Meeting Including the New Horizons Forum and Aerospace Exposition
4 - 7 January 2010, Orlando, Florida

AIAA 2010-535

Transient growth of a Mach 5.92 flat-plate boundary layer

Xiaowen Wang * **and Xiaolin Zhong** †
Mechanical and Aerospace Engineering Department
University of California, Los Angeles, California 90095

Abstract

The laminar-turbulent transition of hypersonic boundary layers has a significant effect on drag calculation and aerothermal analysis of hypersonic vehicles. Surface roughness has been shown to have profound effects on boundary layer transition. Recent research has shown that one possible explanation to roughness induced bypass transition is the transient growth theory. However, there has been very few direct numerical simulation studies on transient growth in hypersonic boundary layers. This paper presents some results in on-going numerical simulation study on the transient growth of a Mach 5.92 flat-plate boundary layer to small three-dimensional surface roughness. The main objective is to study the effects of nonparallel flow and spanwise wave on transient growth. The freestream flow conditions are the same as those used in our previous study [1]. The responses of the boundary layer to surface roughness are computed by solving three-dimensional Navier-Stokes equations with a fifth-order shock-fitting method and a Fourier collocation method. The numerical results show that no transient growth is observed when surface roughness is located in parallel flow region, which indirectly demonstrates that nonparallel flow effects enhance transient growth. It is also shown that surface roughness with a smaller spanwise wave number is more efficient in inducing disturbances with respect to energy norm.

1 Introduction

The laminar-turbulent transition of the boundary-layer flows has a significant effect on drag calculation and aerothermal design of hypersonic vehicles, because a turbulent boundary layer generates much higher shear stress and heat flux to the wall surface than a laminar one. In order to predict and control boundary-layer transition, extensive studies have been carried out to investigate transition mechanisms. Recent research has shown that one possible explanation to roughness induced bypass transition is the transient growth theory [2, 3]. Transient growth arises through the non-orthogonal nature of the Orr-Sommerfeld eigenfunctions and the Squire eigenfunctions. Weak transient growth provides a higher initial amplitude for modal growth whereas strong transient growth can lead to secondary instabilities and breakdown to turbulence right after the receptivity process.

After decades of research, surface roughness has been shown to have profound effects on boundary layer transition. By solving the nonlinear parabolized stability equations (PSE), Bertolotti [4] studied the response of vortices over a plate to surface roughness and wall blowing-suction for an incompressible flow, where the initial vortices were also generated by surface roughness or wall blowing-suction. The results on a flat plate showed that the vortex decayed as $\sqrt{1/x}$ when flowing over streamwise aligned surface roughness, and grew as $\sqrt{x}$ when flowing over a corresponding streamwise aligned variation of wall blowing-suction. The growth of vorticity could be much larger with the presence of surface roughness or wall blowing-suction with both streamwise and spanwise periodicity. On a concave plate, the vortex develops into a Görtler vortex. Choudhari [5] studied the roughness-induced stationary and nonstationary vortices in three-dimensional, incompressible boundary layers over a sweep wing, where nonstationary vortices were induced with the presence of freestream acoustic disturbances. The effects of acoustic-wave orientation and different types of roughness geometries were considered. It was found that maximum receptivity occurred when the velocity fluctuation of acoustic disturbance was aligned with the wave-number vector of nonstationary vortex mode. Gaster et al. [6] measured the velocity disturbance in a flat plate boundary layer induced by a three-dimensional shallow bump oscillating at a frequency of 2 Hz. It was observed that the intensity of velocity

*Research Associate, Mechanical and Aerospace Engineering Department, AIAA Member.
†Professor, Mechanical and Aerospace Engineering Department, AIAA Associate Fellow.

disturbance reached its maximum near $\eta = 2$ at a location about 100 boundary-layer thickness downstream of the bump. They also noticed a small secondary peak in the spanwise spectrum near the bump. Bakchinov et al. [7] studied the stability of an incompressible boundary layer over a flat plate. The experiments were carried out in a low speed wind tunnel. Inside the boundary layer, roughness elements were arranged in spanwise direction to generate stationary streamvise vortices. Small amplitude travelling waves were introduced to the boundary layer on top of the steady vortices. According to their results, the maximum amplification of wave amplitude was found at a wall-normal position where the mean streamwise velocity was equal to wave phase velocity. Joslin and Grosch [8] computed the disturbance velocity field downstream of a shallow bump in a laminar boundary layer by direct numerical simulation of incompressible Navier-Stokes equations. The flow conditions in their simulation was the same as the experimental parameters of Gaster et al. [6]. According to the simulation results, modal growth and decay trends of velocity disturbance were consistent with Gaster et al.'s experimental measurements.

Hanifi et al. [9] investigated transient growth phenomena of boundary-layer flows with a series of Mach numbers from 0.1 to 4.5 using spectral collocation method. They found that maximum transient growth increased with Mach number and could be scaled with the square of local Reynolds number. Andersson et al. [10] numerically calculated the maximum transient growth for steady disturbances and concluded that optimal disturbances consisted of streamwise vortices. They also found that maximum transient growth scaled linearly with the distance from the leading edge. Bottaro and Zebib [11] numerically investigated the formation and growth of spatial G$\ddot{o}$rtler vortices induced by wall roughness. In all naturally developing cases, the average spanwise wavelengths of vortices were close to those of optimal disturbances predicted by LST. Collis and Lele [12] numerically investigated the formation of stationary crossflow vortices in a three-dimensional boundary layer due to surface roughness near the leading edge of a swept wing. The results showed that convex surface curvature enhanced receptivity while non-parallel effects strongly reduced the initial amplitude of stationary crossflow vortices. Reshotko [13] investigated the spatial transient growth by examining examples including Poiseuille flow, hypersonic blunt body paradox, and distributed roughness effects. It was demonstrated that transient growth arised through the coupling between slightly damped, highly oblique T-S and Squire modes. Transient growth thoery offered an explanation for bypass transition, especially for roughness-induced transition.

Tumin and Reshotko [14] proposed a spatial theory for the linear transient growth in a parallel boundary layer. Based on the fact that the spatial development of disturbances downstream of a source could be presented as a sum of decaying eigenmodes and T-S like instability waves, they evaluated the optimal transient growth by applying a standard optimization procedure. The results indicated that the optimal disturbances for transient growth was stationary streamwise vortices. Later, Tumin and Reshotko [15] evaluated optimal disturbances in compressible boundary layers including the nonparallel flow effects. Similarly, the optimal disturbances corresponded to steady counter-rotating streamwise vortices. It was also shown that there was an optimal spacing of the streamwise vortices and an optimal location for their excitation. In order to evaluate the optimal-disturbance theories, White [16] investigated the transient growth of a flat plate boundary layer to spanwise roughness array. The results showed quantitative differences between experimental measurements and theoretical predictions, which did indicate that realistic stationary disturbances could exhibit significant nonoptimal behavior. White and Ergin [17] further studied the receptivity and transient growth of a Blasius boundary layer to roughness-induced disturbances, where the initial disturbances were generated by a spanwise array of roughness elements. In experiments, detailed information on the disturbances and the transient growth was measured using hotwire instruments. The results indicated that energy associated with the roughness-induced disturbances could be scaled with the roughness-based Reynolds number for values as high as 119. Fransson et al. [18] experimentally and theoretically investigated the transient growth of stationary streamwise streaks in a flat plate boundary layer. The stable laminar streaks was periodic in spanwise direction and was generated by a spanwise periodic array of small cylindrical roughness elements. The results showed that the maximum transient growth was mainly determined by the height of roughness elements.

White et al. [19] investigated the effects of the amplitude and diameter of cylindrical roughness elements on transient growth features. Their experimental results showed that energy of stationary disturbances varied as Re_k^2, the square of roughness-based Reynolds number, and the qualitative nature of transient growth strongly depended on the roughness diameter. Choudhari and Fischer [20, 21] examined the roughness-induced transient growth in a laminar boundary layer due to a spanwise periodic array of circular disks at the surface. The effects of roughness height, size, and shape on the transient growth were also explored. Their numerical simulation results indicated that energy levels of the dominant stationary disturbances were consistent with the Re_k^2 scaling of White et al. [19]. Spontaneous vortex shedding behind the roughness array was identified for sufficiently large roughness heights. Tumin [22] solved the receptivity problem of compressible boundary layers to three-dimensional

wall perturbations by using a biorthogonal eigenfunction system. In case of receptivity to roughness elements, a small height hump was considered. The results showed that there were counter rotating streamwise vortices, streaks at both sides of the hump, and a wake region downstream from the hump. In supersonic boundary layers, there existed large amplitude perturbations near the Mach waves generated by roughness elements. Recently, Downs III et al. [23] experimentally studied transient disturbances generated by random distributed roughness. Three test configurations were considered corresponding to roughness-based Reynolds numbers of 164, 227, and 301. All three configurations exhibited transient growth but transition was observed in the configuration of highest surface roughness. Tumin [24] studied the nonparallel flow effects on roughness-induced disturbances in a subsonic flat-plate boundary layer. It was found that nonparallel flow effects lead to lower velocity and higher temperature in the wake.

According to the brief review of previous researches, there has been very few direct numerical simulation (DNS) studies on transient growth in hypersonic boundary layers. In a previous DNS study, we [1] studied the receptivity of a Mach 5.92 flow over a flat plate to three-dimensional surface roughness and the effect of spanwise wave number on the receptivity. The results showed that counter rotating streamwise vortices and transient growth are induced by surface roughness. However, transient growth was generally weak. In this paper, the transient growth of a Mach 5.92 flat-plate boundary layer to small three-dimensional surface roughness is further studied, mainly focusing on the effects of nonparallel flow and spanwise wave number on transient growth. Two-dimensional steady flow over the flat plate is firstly achieved by solving compressible Navier-Stokes equations with a combination of a fifth-order shock-fitting method and a second-order TVD scheme. The three-dimensional steady flow is directly extended from two-dimensional base flow due to the fact that the base flow over the flat plate is independent of spanwise coordinate. The subsequent responses of the hypersonic boundary layer to small surface roughness are simulated by solving three-dimensional Navier-Stokes equations with a fifth-order shock-fitting method and a Fourier collocation method.

2 Governing Equations and Numerical Methods

In current studies, a Mach 5.92 flow over a flat plate as shown in Fig. 1 is considered. The flow is assumed to be thermally and calorically perfect. The governing equations are the full Navier-Stokes equations in the conservative form, i.e.,

$$\frac{\partial \vec{U}^*}{\partial t^*} + \frac{\partial}{\partial x_1^*}(\vec{F}_{1i}^* + \vec{F}_{1v}^*) + \frac{\partial}{\partial x_2^*}(\vec{F}_{2i}^* + \vec{F}_{2v}^*) + \frac{\partial}{\partial x_3^*}(\vec{F}_{3i}^* + \vec{F}_{3v}^*) = 0 \tag{1}$$

where the superscript "$*$" represents the dimensional variables. $\vec{U}^*$ is a vector containing the conservative variables of mass, momentum, and energy, i.e.,

$$\vec{U}^* = \{\rho^*, \rho^* u_1^*, \rho^* u_2^*, \rho^* u_3^*, e^*\} \tag{2}$$

The flux vector in Eq. (1) is divided into its inviscid and viscous components, because the two components are discretized with different schemes. The components, $\vec{F}_{1i}^*$, $\vec{F}_{2i}^*$, $\vec{F}_{3i}^*$, are inviscid flux vectors whereas $\vec{F}_{1v}^*$, $\vec{F}_{2v}^*$, and $\vec{F}_{3v}^*$ are viscous flux vectors. The flux vectors can be expressed as

$$\vec{F}_{ji}^* = \begin{bmatrix} \rho^* u_j^* \\ \rho^* u_1^* u_j^* + p^* \delta_{1j} \\ \rho^* u_2^* u_j^* + p^* \delta_{2j} \\ \rho^* u_3^* u_j^* + p^* \delta_{3j} \\ u_j^*(e^* + p^*) \end{bmatrix}, \quad \vec{F}_{jv}^* = \begin{bmatrix} 0 \\ -\tau_{1j}^* \\ -\tau_{2j}^* \\ -\tau_{3j}^* \\ -\tau_{1j}^* u_1^* - \tau_{2j}^* u_2^* - \tau_{3j}^* u_3^* + k^* \frac{\partial T^*}{\partial x_j^*} \end{bmatrix} \tag{3}$$

with $j \in \{1, 2, 3\}$. In Eq. (3), δ_{ij} $(i = 1, 2, 3)$ is the Kronecker Delta function. In the perfect gas assumption, pressure and energy are given by

$$p^* = \rho^* R^* T^* \tag{4}$$

$$e^* = \rho^* c_v^* T^* + \frac{\rho^*}{2}(u_1^{*2} + u_2^{*2} + u_3^{*2}) \tag{5}$$

where c_v^* is the specific heat at constant volume. For compressible Newtonian flow, the viscous stress tensor can be written as:

$$\tau_{ij}^* = \mu^* \left(\frac{\partial u_i^*}{\partial x_j^*} + \frac{\partial u_j^*}{\partial x_i^*} \right) - \frac{2}{3}\mu^* \left(\frac{\partial u_1^*}{\partial x_1^*} + \frac{\partial u_2^*}{\partial x_2^*} + \frac{\partial u_3^*}{\partial x_3^*} \right) \delta_{ij} \tag{6}$$

with $i, j \in \{1, 2, 3\}$. In the simulation, the viscosity coefficient, μ^*, and the heat conductivity coefficient, k^*, are calculated using the Sutherland's law together with a constant Prandtl number, Pr. They are both functions of temperature only.

$$\mu^* = \mu_r^* \left(\frac{T^*}{T_r^*} \right)^{3/2} \frac{T_r^* + T_s^*}{T^* + T_s^*} \tag{7}$$

$$k^* = \frac{\mu^* c_p^*}{Pr} \tag{8}$$

where $\mu_r^* = 1.7894 \times 10^{-5}$ Ns/m^2, $T_r^* = 288.0$ K, $T_s^* = 110.33$ K, and c_p^* is the specific heat at constant pressure. Dimensional flow variables are non-dimensionalized by freestream parameters. Specifically, density ρ^*, temperature T^*, velocities u_1^*, u_2^*, u_3^*, and pressure p^* are non-dimensionalized by ρ_∞^*, T_∞^*, u_∞^*, and $\rho_\infty^* u_\infty^{*2}$. Furthermore, x_1^* and x_3^* is non-dimensionalized by unit length in meter, whereas x_2^* is non-dimensionalized by Blasius boundary-layer thickness, $\sqrt{\mu_\infty^* x_1^* / \rho_\infty^* u_\infty^*}$. Referring to the coordinate system shown in Fig. 1, x_1^*, x_2^*, and x_3^* are x^*, y^*, and z^*, respectively. The three variables, u_1^*, u_2^*, and u_3^*, are velocities in streamwise, wall-normal, and spanwise directions.

The high-order shock-fitting finite difference method of Zhong [25] is used to solve the governing equations in a domain bounded by the bow shock and the flat plate. In orther words, the bow shock is treated as a boundary of the computational domain. The Rankine-Hugoniot relation across the shock and a characteristic compatibility relation coming from downstream flow field are combined to solve the flow variables behind the shock. The shock-fitting method makes it possible for the Navier-Stokes equations to be spatially discretized by high-order finite difference methods. Specifically, a fifth-order upwind scheme is used to discretize the inviscid flux derivatives. Meanwhile, a sixth-order central scheme is used to discretize the viscous flux derivatives. For three-dimensional simulations, flux derivatives of $\vec{F}_{3i}^*$ and $\vec{F}_{3v}^*$ in spanwise direction are calculated by Fourier collocation method to achieve high accuracy. By using the shock-fitting method, the interaction between the bow shock and perturbations induced by wall disturbances is solved as a part of solutions with the position and velocity of the shock front being taken as dependent flow variables. Temporal integration of the governing equations is obtained using Runge-Kutta method. One can find more details of the numerical methods in our previous paper [1].

3 Flow Conditions and Linear Boundary Condition Transfer

Freestream conditions of the currently studied flow are as follows,

$$M_\infty = 5.92\,, \qquad T_\infty^* = 48.69\text{K}\,,$$
$$p_\infty^* = 742.76\text{Pa}\,, \qquad Pr = 0.72\,,$$
$$Re_\infty^* = 13 \times 10^6/\text{m}$$

The dimensional coordinate, x^* as shown in Fig. 1, can be converted to local Reynolds number by

$$Re_x = Re_\infty^*\ x^* \tag{9}$$

where Re_∞^* is the unit Reynolds number defined as

$$Re_\infty^* = \rho_\infty^* u_\infty^* / \mu_\infty^* \tag{10}$$

In LST studies of boundary-layer flows, the Reynolds number based on Blasius boundary-layer thickness, L^*, is generally used. They are expressed as

$$R = \frac{\rho_\infty^* u_\infty^* L^*}{\mu_\infty^*}, \quad L^* = \sqrt{\frac{\mu_\infty^* x^*}{\rho_\infty^* u_\infty^*}} \tag{11}$$

Hence, the relation between R and local Reynolds number Re_x is given by

$$R = \sqrt{Re_x} \tag{12}$$

In smooth region, the wall is adiabatic, and the physical boundary condition of velocity on the flat plate is the no-slip condition. When small surface roughness is introduced on the flat plate, boundary conditions of temperature and velocities on the rough surface are transferred to original smooth surface by linear extrapolation due to small height of roughness element. Figure 2 schematically shows the linear boundary condition transfer of streamwise velocity, where the blue arrows stand for the streamwise velocity boundary conditions for points A and B on original smooth surface. Inlet conditions are specified, while high-order extrapolation is used for outlet conditions because the flow is hypersonic at the exit boundary except a small region near the flat plate.

Due to the existence of small roughness, the wall surface changes from $y^* = 0$ to $y^* = \epsilon\hbar^*(x^*, z^*)$, where $y^* = 0$ stands for original smooth surface. The function, $\hbar^*(x^*, z^*)$, represents the profile of roughness elements. The parameter, ϵ, is used to adjust the height. The physical no-slip conditions of velocity on the rough surface are

$$\begin{cases} u^*(x^*, \epsilon\hbar^*(x^*, z^*), z^*) = 0 \\ v^*(x^*, \epsilon\hbar^*(x^*, z^*), z^*) = 0 \\ w^*(x^*, \epsilon\hbar^*(x^*, z^*), z^*) = 0 \end{cases} \tag{13}$$

Under the assumption of small-height roughness elements, boundary conditions on the rough wall can be transferred to original smooth surface by linear extrapolation, i.e.,

$$\begin{cases} u^*(x^*, 0, z^*) = -\epsilon\hbar^*(x^*, z^*)\frac{\partial u^*}{\partial y^*} \mid_{y^*=0} \\ v^*(x^*, 0, z^*) = -\epsilon\hbar^*(x^*, z^*)\frac{\partial v^*}{\partial y^*} \mid_{y^*=0} \\ w^*(x^*, 0, z^*) = -\epsilon\hbar^*(x^*, z^*)\frac{\partial w^*}{\partial y^*} \mid_{y^*=0} \end{cases} \tag{14}$$

The adiabatic temperature condition used on rough surface is expressed as

$$\frac{\partial T^*(x^*, \epsilon\hbar^*(x^*, z^*), z^*)}{\partial y^*} = 0 \tag{15}$$

Similarly, the temperature condition can be transferred to original smooth surface as follows:

$$\frac{\partial T^*(x^*, 0, z^*)}{\partial y^*} = -\epsilon\hbar^*(x^*, z^*)\frac{\partial^2 T^*}{\partial y^{*2}} \mid_{y^*=0} \tag{16}$$

In Eqs. (14) and (16), all derivatives on the right-hand-side of equations are calculated from the steady flow over smooth flat plate.

For the roughness elements considered in current paper, the function of $\hbar^*(x^*, z^*)$ is defined as

$$\hbar^*(x^*, z^*) = \hbar^*(l)\cos(\beta^* z^*) \tag{17}$$

where β^* is the spanwise wave number. The function $\hbar^*(l)$ and the variable l are defined as

$$\hbar^*(l) = (20.25l_4^5 - 35.4375l_4^4 + 15.1875l_4^2)/2.45688 \tag{18}$$

$$l = 0.620287 \times \begin{cases} 2(x^* - x_i^*)/(x_e^* - x_i^*) \\ 2(x_e^* - x^*)/(x_e^* - x_i^*) \end{cases} \tag{19}$$

where x_i^* and x_e^* are the coordinates of the leading and trailing edges of the roughness elements in streamwise direction. The constant, 2.45688, is the value of $\hbar^*(l)$ at $l = 0.620287$, which is used to normalize the profile function. Figure 3 shows the profile function $\hbar^*(l)$ and the variable l of the roughness element in streamwise direction. It is clearly shown that both $\hbar^*(l)$ and l are symmetric within the roughness region. And the height of surface roughness reaches its maximum at the center.

4 Results and Discussions

Two-dimensional steady flow over the flat plate is firstly simulated by solving the two-dimensional compressible Navier-Stokes equations with a combination of a fifth-order shock-fitting finite difference method and a second-order TVD scheme. The three-dimensional steady flow is directly extended from two-dimensional one due to the fact that the steady flow on the flat plate is independent of spanwise coordinate. Since we already have two-dimensional steady flow, such treatment is much more efficient than directly solving 3-D Navier-Stokes equations with uniform initial conditions.

In the leading edge region, there exists a singular point at the tip of the flat plate, which will introduce numerical instability if the fifth-order shock-fitting method is used to simulate the flow. Therefore, a second-order TVD scheme used by Zhong and Lee [26] is applied to simulate the steady base flow in a small region including the leading edge. The computational domain for the fifth-order shock-fitting method starts at $x^* = 0.0025$ m and ends at $x^* = 0.879$ m, corresponding to $R = 180.28$ and $R = 3380.38$, respectively. The computational domain for the second-order TVD scheme starts at $x^* = -0.0005$ m and ends at $x^* = 0.0035$ m. Three sets of grid structures are used to check the grid independence of the numerical results. Figure 4 compares the density distributions in wall-normal direction. In this figure, the density distributions are evaluated at $x^* = 0.0025$ m, the initial location of the first zone. It shows that density distribution on 201×176 mesh agrees well with that on 241×181 mesh whereas it has significant discrepancies with that on 161×101 mesh. This figure indicates that the grid structure of 201×176 is fine enough to ensure the grid independence of numerical results. However, the grid structure of 161×101 is too coarse to achieve spatially converged numerical results.

Figures 5(a) and 5(b) shows pressure contours of steady base flow computed by the fifth-order shock-fitting method. In Fig. 5(a), the upper boundary of flow field represents bow shock induced by displacement thickness of the boundary layer. The lower boundary is the flat plate. A part of pressure contours from $x^* = 0.33$ m to $x^* = 0.36$ m ($R = 2071.23$ to $R = 2163.33$) is amplified in Fig. 5(b) to show clearly pressure distributions within the boundary layer. It is noticed that pressure is approximately a constant across the boundary layer and along the Mach lines, which is consistent with boundary layer theory and inviscid supersonic aerodynamics. At a fixed location (constant x^*), pressure behind the shock is higher than that on flat plate due to the existence of bow shock.

Figure 6 shows bow shock position and distribution of Mach number behind the shock. In this figure, a straight line tangential to shock near the leading edge is plotted helping to illustrate that the shock is not a straight line. Decrease of shock angle from upstream to downstream indicates that the shock becomes weaker downstream. The dramatic increase of Mach number near the leading edge is also due to interaction between viscous boundary layer and inviscid outer flow. After $x^* = 33$ mm ($R = 654.98$), intensity of viscous-inviscid interaction decreases quickly with blow shock moving away from the boundary layer. Mach number behind the shock approaches a constant downstream. The increase of Mach number also indicates that bow shock becomes weaker from upstream to downstream. The accuracy of the steady base flow has been validated by comparisons with Maslov et al.'s experimental measurements [27] and the self-similar boundary-layer solution. One can refer to our previous papers for the detailed results on the steady flow [1, 28].

In compressible boundary layer, a specific energy norm is defined to measure the strength of transient growth [9, 14], which is defined as

$$E_k = (\vec{q}, \vec{q})_2 = \int_0^\infty \vec{q}^T M \vec{q} dy \tag{20}$$

where the perturbation amplitude vector, $\vec{q}$, and the diagonal matrix, M, are expressed as

$$\vec{q} = (\hat{u}, \hat{v}, \hat{\rho}, \hat{T}, \hat{w})^T \tag{21}$$

$$M = diag[\rho, \rho, T/(\gamma \rho Me^2), \rho/(\gamma(\gamma-1)TMe^2), \rho] \tag{22}$$

In current paper, the same energy norm is evaluated. The integral in Eq. (20) is numerical calculated across the boundary layer using a mid-point rule.

According to the model of surface roughness, boundary conditions of temperature and velocities on rough surface are linearly transferred to original smooth surface using Eqs. (14) and (16). In order to keep valid the linear

extrapolation of boundary conditions, the height of surface roughness is fixed at $\epsilon = 1.0 \times 10^{-5}$ m, which has been proved to be small enough [1]. The location of roughness element is defined by x_i^* and x_e^* at $z^* = 0$ plane as

$$x_i^* = 0.1332\text{m}, x_e^* = 0.1398\text{m} \tag{23}$$

Compared with the roughness elements considered in our previous study [1], roughness elements considered here is far downstream of the leading edge, where the flow is parallel as has been demonstrated by Maslov et al. [27].

4.1 Nonparallel flow effects

In current paper, surface roughness is located downstream where the flow is parallel. Whereas in our previous study [1], roughness element is very close to the leading edge, nonparallel flow effects are important there. To study the nonparallel flow effects, we try to compare results in current paper to those in our previous one. Therefore, two test cases of surface roughness with different spanwise wave number are considered in this section:

- Case 1: $\beta = 0.3$
- Case 2: $\beta = 0.1$

where the wave number is nondimensionalized by the scale of boundary-layer thickness at the center of roughness ($x^* = 0.1565$ m). These two spanwise wave number had been tested in our previous study. Here, surface roughness is parallel to the leading edge of the flat plate, as shown in Fig. 1.

Figure 7 shows the boundary conditions used in the roughness region at $z^* = 0$ plane in case 1. It shows that, outside the roughness region, velocity disturbances are zero whereas temperature disturbance is nonzero due to the adiabatic condition. It is also noticed that wall-normal velocity disturbance is close to zero (order of 10^{-9}), which indicates that flow is parallel at this location. Similar results is obtained in case 2. Figure 8 compares the energy norm along the flat plate in case 1 with the counterpart calculated in our previous paper [1]. The figure shows that roughness element located upstream is more efficient in exciting disturbances. However, no transient growth is observed downstream of the roughness in this figure. To check transient growth, the two energy norms downstream of the roughness are replotted in a smaller range, as shown in Figs. 9 and 10, respectively. Figure 9 shows weak transient growth around $x^* = 0.04$ m. However, energy norm in Fig. 10 keeps decreasing in the computational domain, no transient growth is observed. It seems that nonparallel flow effects enhance transient growth.

Figure 11 compares the energy norm along the flat plate in case 2 with the counterpart calculated in our previous paper [1]. Similarly, the figure shows that roughness element located upstream is more efficient in exciting disturbances. For the upstream surface roughness, transient growth of the disturbances is clearly shown. However, no transient growth is observed in current computation domain of case 2. The energy norm keeps decreasing downstream of the roughness. Figures 8 and 11 indirectly demonstrate that nonparallel flow effects enhance transient growth. In order to inducing strong transient growth, surface roughness should be aligned near the leading edge of the flat plate.

4.2 Effect of spanwise wave number

Spanwsie wave number of the surface roughness has a critical effect on transient growth. In this section, six cases of numerical simulations are carried out for surface roughness with different spanwise wave numbers. The spanwise wave number is tabulated in Table 1, together with the corresponding computational domain in which the numerical simulation has completed. In this table, all spanwise wave number are nondimensionalized by the scale of boundary-layer thickness at the center of roughness ($x^* = 0.1565$ m).

Figure 12 compares the vector of $w\prime$ and $v\prime$ perturbations in the (y^*, z^*) plane for the six cases of numerical simulations at $x^* = 0.1458$ m ($R = 1435.08$), a location right after the surface roughness. In this figure, the labels (a) to (f) represent the numerical simulation results of cases 1 to 6. These figures qualitatively show that counter-rotating streamwise vortices are induced by surface roughness. With the spanwise wave number decreasing or spanwise wave length increasing from Fig. 12(a) to Fig. 12(f) , the vortices are moving towards the wall, and spanwise velocity component, $w\prime$, is decreasing.

Figure 13 compares the vorticity distribution in streamwise direction at $z^* = 0$ plane in cases 1 to 6. It shows that, from cases 1 to 4, surface roughness with a smaller spanwise wave number is more efficient in generating streamwise vorticity. However, this trend is inversed for case 5 and 6. These results come from the combination effect of the vortex movement towards the wall and the decrease of spanwise velocity component. With the vortex

moves near the wall, larger vorticity will be induced on the wall and in the boundary layer. On the other hand, with the spanwise velocity component decreasing, the steamwise vortices weaken, leading to a smaller vorticity on the wall and in the boundary layer. Figure 14 compares the energy norm distribution along the flat plate near surface roughness in cases 1 to 6. It shows that surface roughness with a smaller spanwise wave number is more efficient in inducing disturbances with respect to energy norm.

Figure 15 compares the energy norm distribution along the flat plate downstream of the surface roughness in cases 1 to 6. It is clearly shown that no transient growth is observed in all six cases of simulations. Compared with the results of our previous research as shown in Fig. 16, one can conclude that surface roughness considered in current paper is far less efficient in inducing transient growth. Again, such results indirectly demonstrate that nonparallel flow effects enhances transient growth.

5 Summary

Recent research has shown that one possible explanation to roughness induced bypass transition is the transient growth theory. However, there has been very few direct numerical simulation studies on transient growth in hypersonic boundary layers. In this paper, the transient growth of a Mach 5.92 flat-plate boundary layer to small three-dimensional surface roughness is further studied, mainly focusing on the effects of non-parallel flow and spanwise wave number on transient growth. Two-dimensional steady flow over the flat plate is firstly achieved by solving compressible Navier-Stokes equations with a combination of a fifth-order shock-fitting method and a second-order TVD scheme. The three-dimensional steady flow is directly extended from two-dimensional base flow due to the fact that the base flow over the flat plate is independent of spanwise coordinate. The subsequent responses of the hypersonic boundary layer to small surface roughness are simulated by solving three-dimensional Navier-Stokes equations with a fifth-order shock-fitting method and a Fourier collocation method.

The numerical results show that no transient growth is observed when surface roughness is located in parallel flow region, which indirectly demonstrates that nonparallel flow effects enhance transient growth. It is also shown that surface roughness with a smaller spanwise wave number is more efficient in inducing disturbances with respect to energy norm. Further studies are needed to study the effects nonparallel flow and spanwise wave number in a longer computational domains.

Acknowledgments

This work was sponsored by the AFOSR/NASA National Center for Hypersonic Research in Laminar-Turbulent Transition and by the Air Force Office of Scientific Research, USAF, under Grants No. FA9550-07-1-0414 and FA9550-04-1-0029, monitored by Dr. John Schmisseur. The views and conclusions contained herein are those of the authors and should not be interpreted as necessarily representingthe official policies or endorsements either expressed or implied, of the Air Force Office of Scientific Research or the U.S. Government.

References

[1] X. Wang and X. Zhong. Receptivity of a Hypersonic Flat-Plate Boundary Layer to Three-Dimensional Surface Roughness. *Journal of Spacecraft and Rockets*, Vol. 45, No. 6, pp. 1165-1175, 2008.

[2] E. Reshotko and A. Tumin. Role of transient growth in roughness-induced transition. *AIAA Journal*, Vol.42, No.4, pp.766-770, 2004.

[3] E. Reshotko. Is Re_θ/Me a meaningful transition criterion ? *AIAA paper 2007-0943*, January 2007.

[4] F. P. Bertolotti. Vortex generation and wave-vortex interaction over a concave plate with roughness and suction. *ICASE Report*, No.93-101, 1993.

[5] M. Choudhari. Roughness-induced generation of crossflow vortices in three-dimensional boundary layers. *Theoretical and Computational Fluid Dynamics*, Vol.6, pp.1-30, 1994.

[6] M. Gaster, C. E. Grosch, and T. L. Jackson. The velocity field created by a shallow bump in a boundary layer. *Physics of Fluids*, Vol.6, No.9, pp.3079-3085, 1994.

[7] A. A. Bakchinov, G. R. Grek, B. G. B. Klingmann, and V. V. Kozlov. Transition experiments in boundary layer with embedded streamwise vortices. *Physics of Fluids*, Vol.7, No.4, pp.820-832, 1995.

[8] R. D. Joslin and C. E. Grosch. Growth characteristics downstream of a shallow bump: Computation and experiment. *Physics of Fluids*, Vol.7, No.12, pp.3042-3047, 1995.

[9] A. Hanifi, P. J. Schmid, and D. S. Henningson. Transient growth in compressible boundary layer flow. *Physics of Fluids*, Vol.8, No.3, pp.826-837, 1996.

[10] P. Andersson, M. Berggren, and D. S. Henningson. Optimal Disturbances and Bypass Transition in Boundary Layers. *Physics of Fluids*, Vol.11, No.1, pp.134-150, 1999.

[11] A. Bottaro and A. Zebib. Görtler vortices promoted by wall roughness. *Fluid Dynamics Research*, Vol.19, pp.343-362, 1997.

[12] S. S. Collis and S. K. Lele. Receptivity to surface roughness near a swept leading edge. *Journal of Fluid Mechanics*, Vol.380, pp.141-168, 1999.

[13] E. Reshotko. Transient growth: A factor in bypass transition. *Physics of Fluids*, Vol.13, No.5, pp.1067-1075, 2001.

[14] A. Tumin and E. Reshotko. Spatial Theory of Optimal Disturbances in Boundary Layers. *Physics of Fluids*, Vol.13, No.7, 2001.

[15] A. Tumin and E. Reshotko. Optimal Disturbances in Compressible Boundary Layers. *AIAA Journal*, Vol. 41, No. 12, 2003.

[16] E. B. White. Transient growth of stationary disturbances in a flat plate boundary layer. *Physics of Fluids*, Vol. 14, No. 12, pp. 4429-4439, 2002.

[17] E. B. White and F. G. Ergin. Receptivity and transient growth of roughness-induced disturbances. *AIAA paper 2003-4243*, June 2003.

[18] J. H. M. Fransson and L. Brandt. Experimental and theoretical investigation of the nonmodal growth of steady streaks in a flat plate boundary layer. *Physics of Fluids*, Vol. 16, No. 10, pp. 3627-3638, 2004.

[19] E. B. White, J. M. Rice, and F. G. Ergin. Receptivity of stationary transient disturbances to surface roughness. *Physics of Fluids*, Vol.17, No.6, Paper No.064109, 2005.

[20] P. Fischer and M. Choudhari. Numerical simulation of roughness-induced transient growth in a laminar boundary layer. *AIAA paper 2004-2539*, June 2004.

[21] M. Choudhari and P. Fischer. Roughness-induced transient growth. *AIAA paper 2005-4765*, June 2005.

[22] A. Tumin, X. Wang, and X. Zhong. Direct numerical simulation and the theory of receptivity in a hypersonic boundary layer. *Physics of Fluids*, Vol. 19, Paper No. 014101, 2007.

[23] R. S. Downs III, E. B. White, and N. A. Denissen. Transient growth and transition induced by random distributed roughness. *AIAA Journal*, Vol. 46, No. 2, 2003.

[24] A. Tumin. Nonparallel flow effects on roughness-induced perturbations in boundary layers. *Journal of Spacecraft and Rockets*, Vol. 45, No. 6, pp. 1176-1184, 2008.

[25] X. Zhong. High-Order Finite-Difference Schemes for Numerical Simulation of Hypersonic Boundary-Layer Transition. *Journal of Computational Physics*, Vol.144, pp. 662-709, 1998.

[26] X. Zhong and T. Lee. Nonequilibrium real-gas effects on disturbance/bow shock interaction in hypersonic flow past a cylinder. *AIAA paper 1996-1856*, January 1996.

[27] A. A. Maslov, A. N. Shiplyuk, A. Sidorenko, and D. Arnal. Leading-edge receptivity of a hypersonic boundary layer on a flat plate. *Jounral of Fluid Mechanics*, Vol.426, pp.73-94, 2001.

[28] X. Wang and X. Zhong. Effect of wall perturbations on the receptivity of a hypersonic boundary layer. *Physics of Fluids*, Vol. 21, No. 4, Paper No. 044101, 2002.

n	β	Start of computational domain(m)	End of computational domain (m)
1	0.4	0.129	0.162
2	0.3	0.129	0.284
3	0.2	0.129	0.254
4	0.1	0.129	0.194
5	0.01	0.129	0.162
6	0.001	0.129	0.162

Table 1: Spanwise wave number and computational domain for the six cases of numerical simulations.

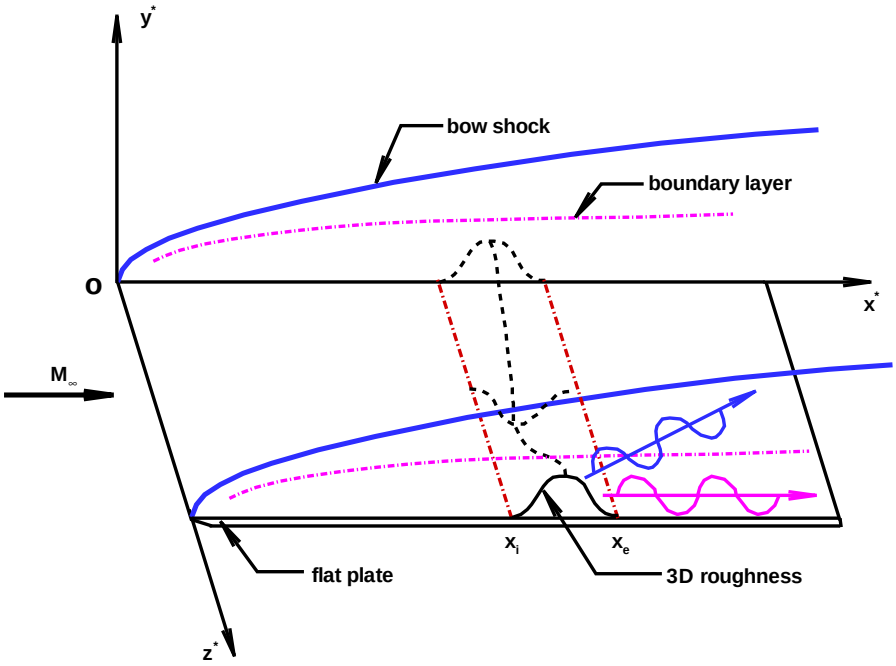

Figure 1: A schematic of the receptivity of the Mach 5.92 flow to three-dimensional surface roughness.

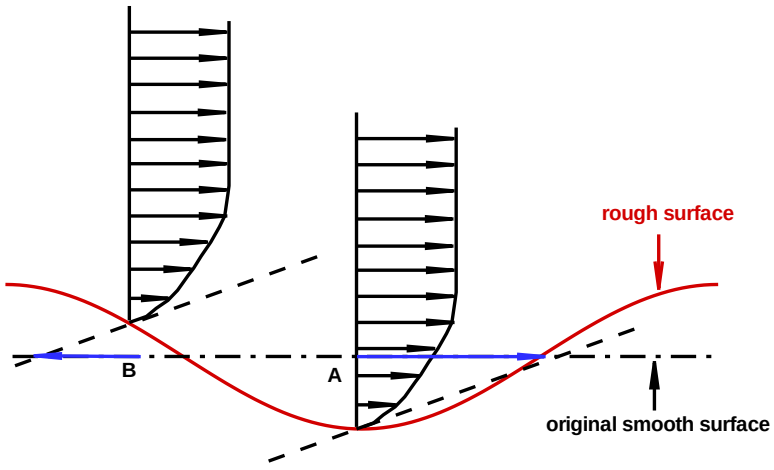

Figure 2: A schematic of linear boundary condition transfer of streamwise velocity for points A and B on original smooth surface.

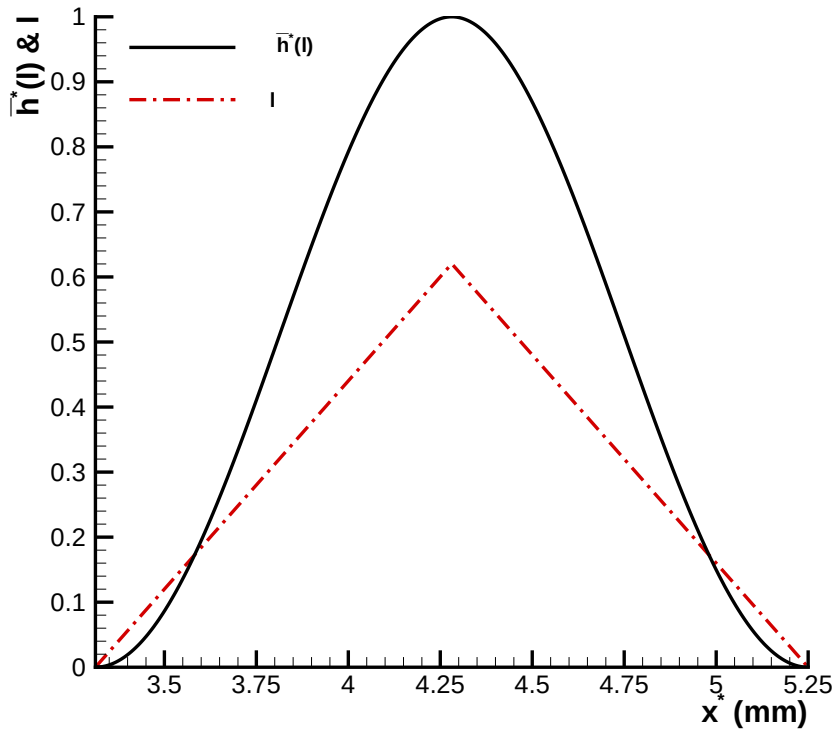

Figure 3: The profile function $\hbar^*(l)$ and the variable l of the roughness element in streamwise direction.

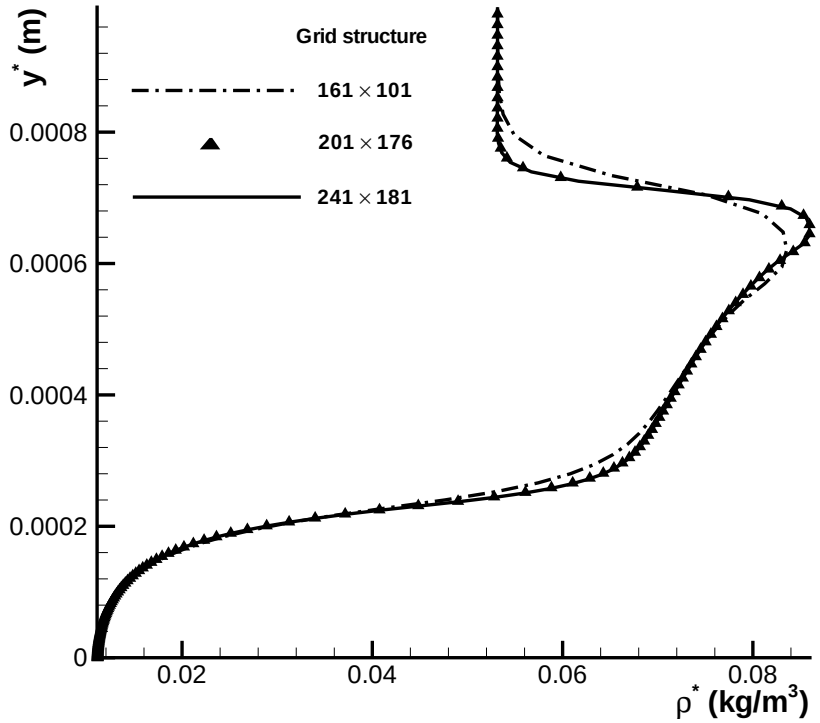

Figure 4: Comparison of density distributions in wall-normal direction at $x^* = 0.0025$ m simulated by second-order TVD scheme based on three sets of grid structures.

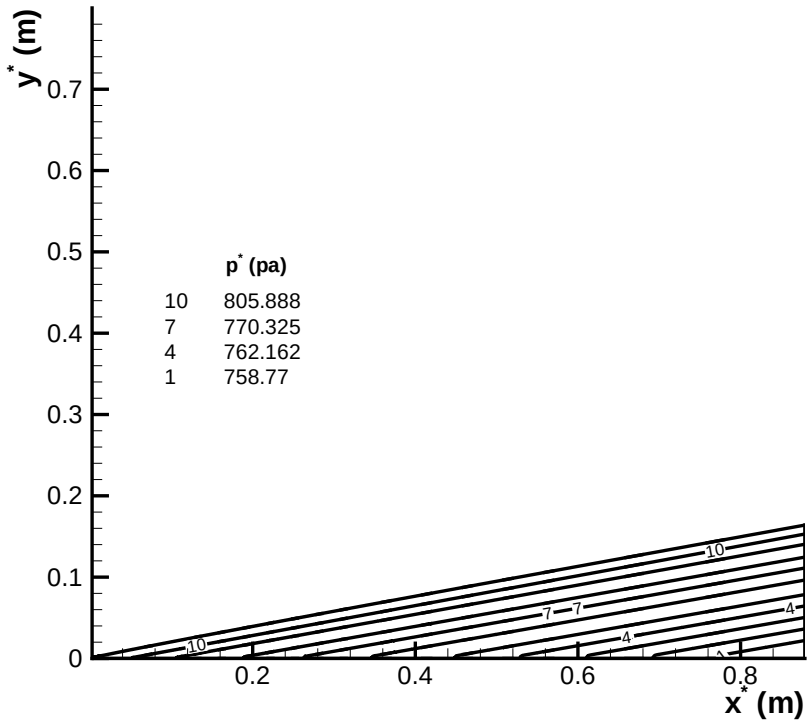

(a)

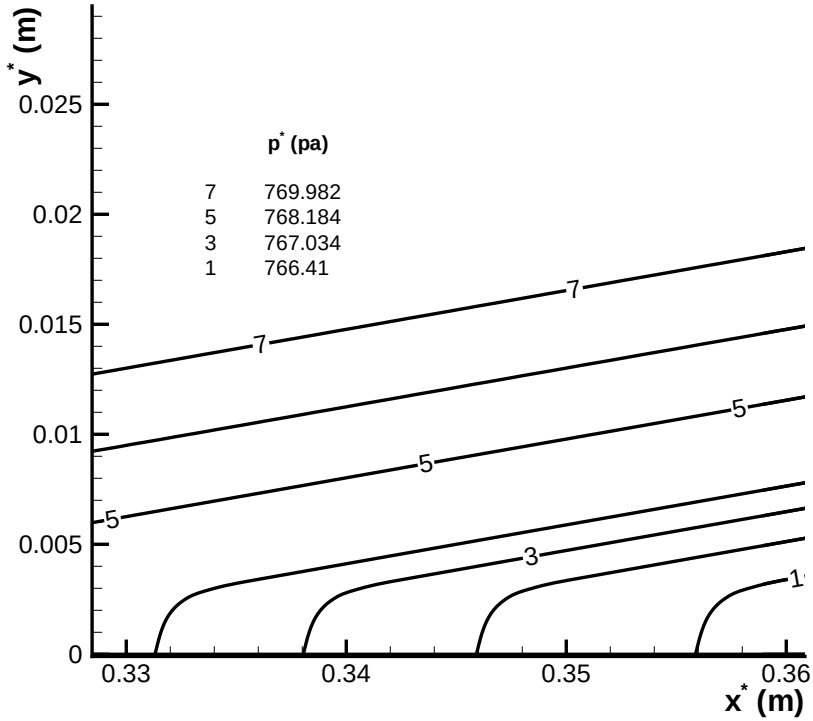

(b)

Figure 5: Pressure contours of steady base flow computed by the fifth-order shock-fitting method.

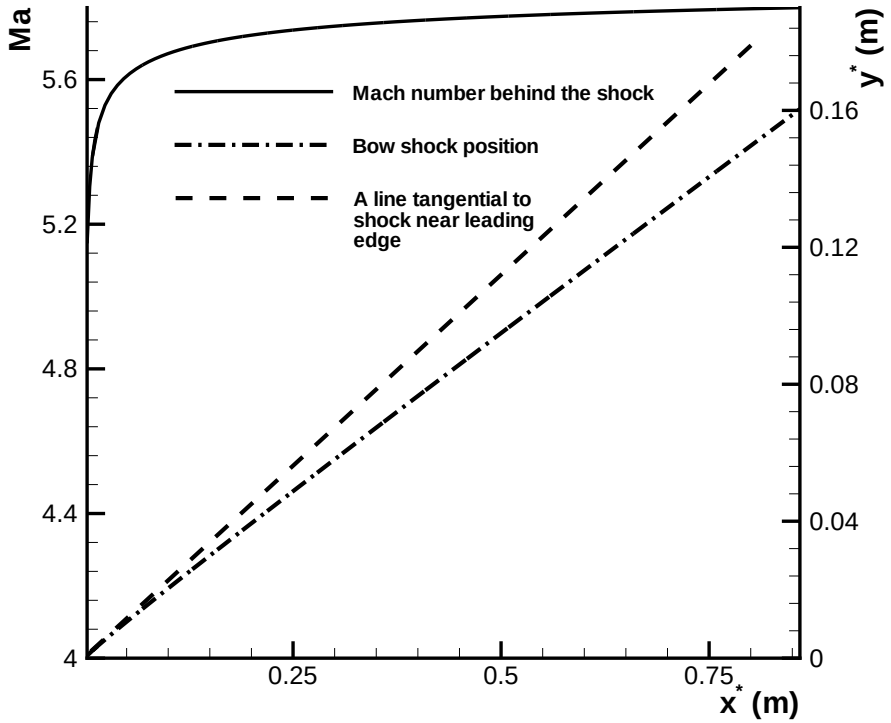

Figure 6: Shock position and distribution of Mach number behind the shock.

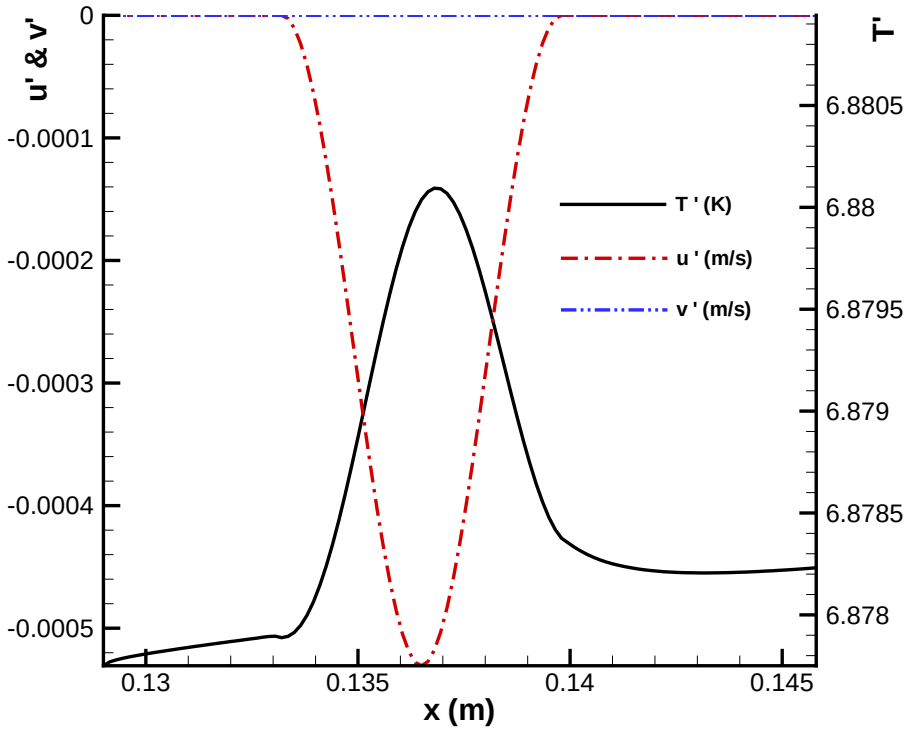

Figure 7: The disturbances enforced on the rough region at $z^* = 0$ plane in case 1 .

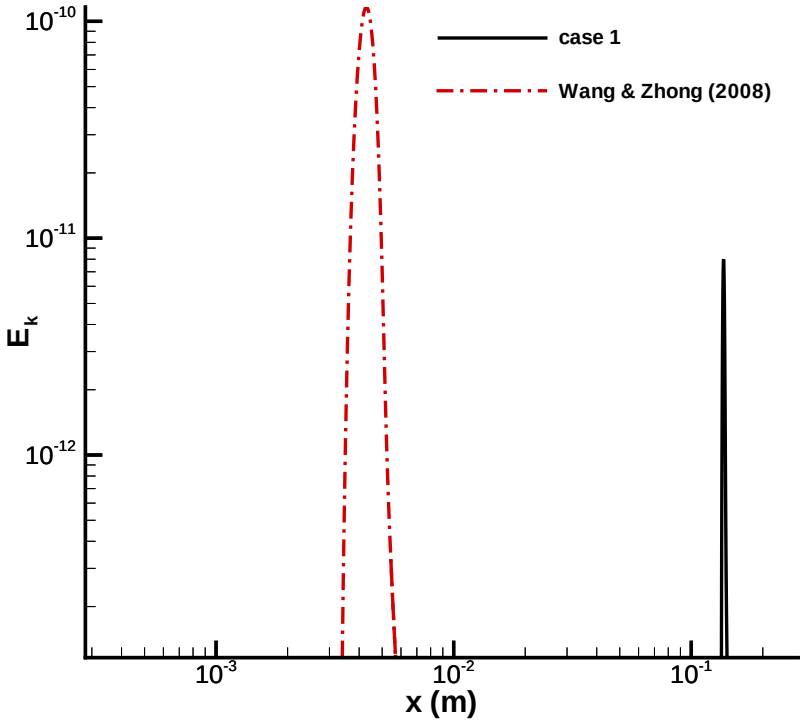

Figure 8: Comparison of energy norm distribution along the flat plate for surface roughness with $\beta = 0.3$.

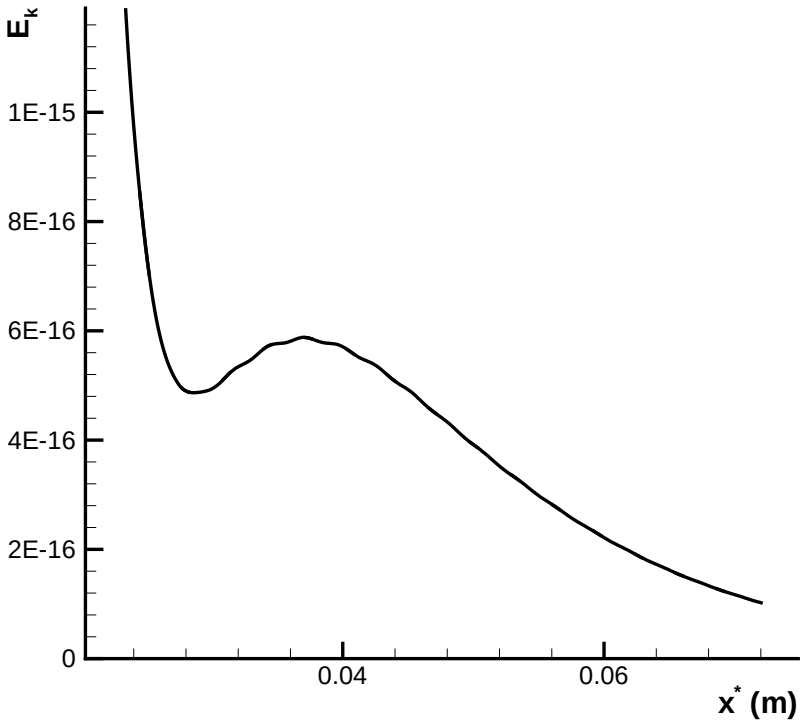

Figure 9: Amplified energy norm distribution along the flat plate for surface roughness with $\beta = 0.3$ [1].

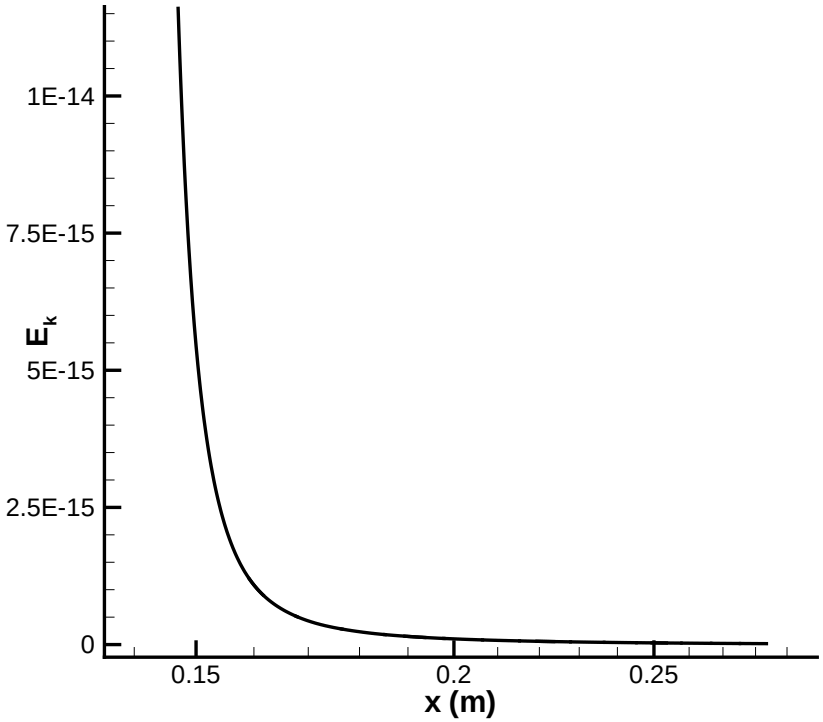

Figure 10: Amplified energy norm distribution along the flat plate for surface roughness with $\beta = 0.3$ in case 1.

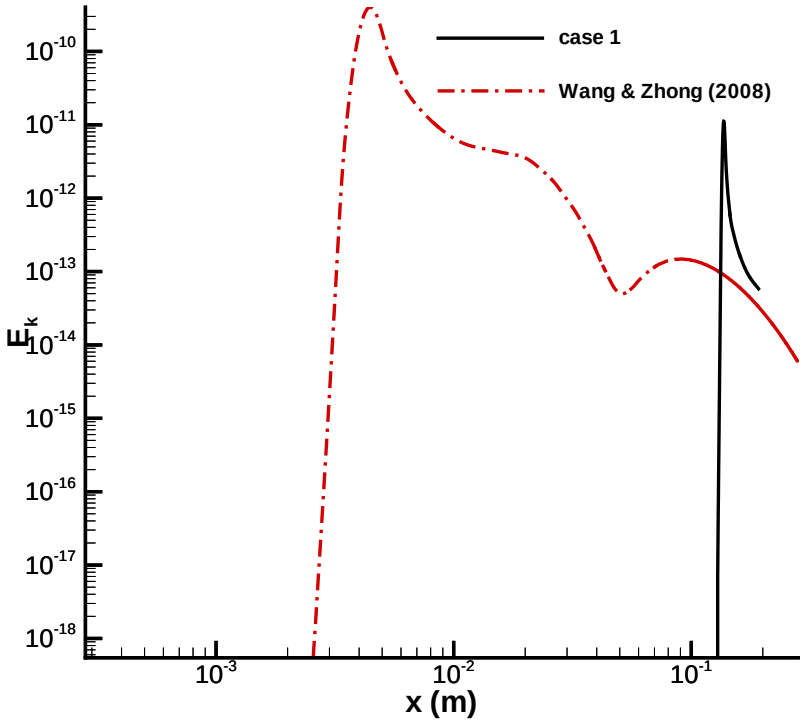

Figure 11: Comparison of energy norm distribution along the flat plate for surface roughness with $\beta = 0.1$.

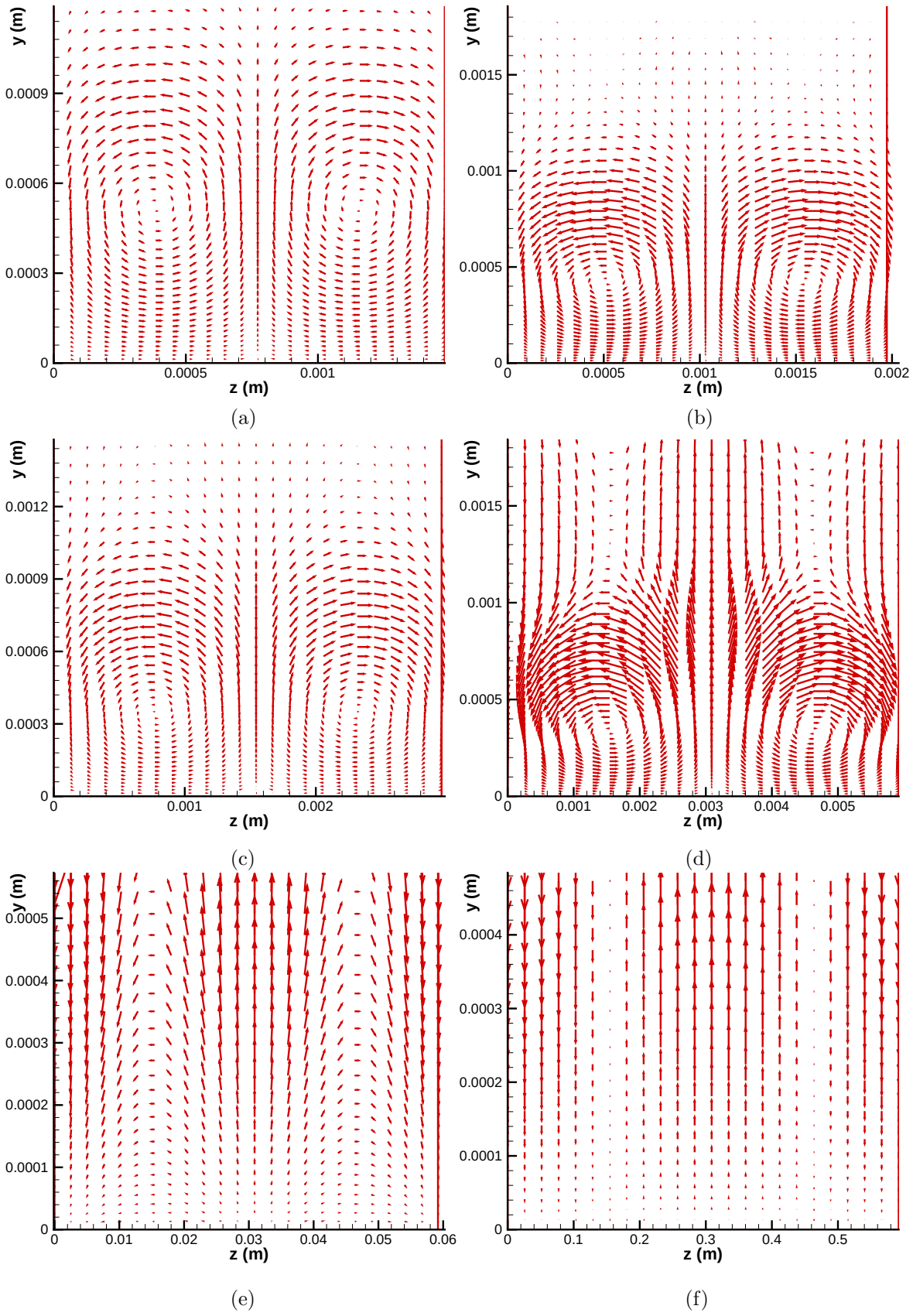

Figure 12: Vector plot of $w\prime$ and $v\prime$ perturbations in the (y^*, z^*) plane at the location of $x^* = 0.1458$ m.

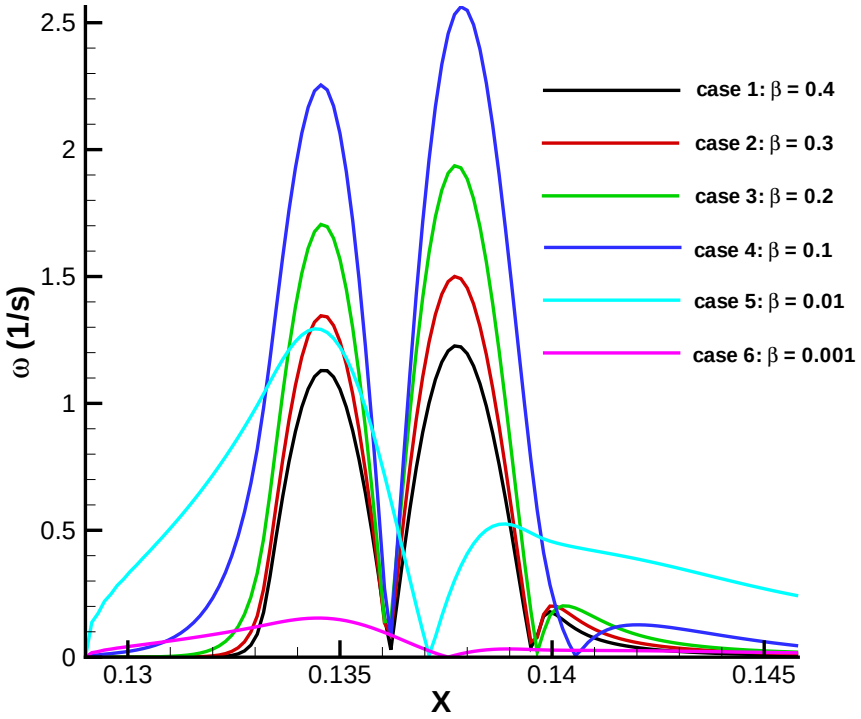

Figure 13: Comparison of the vorticity distribution in streamwise direction at $z^* = 0$ plane in cases 1 to 6.

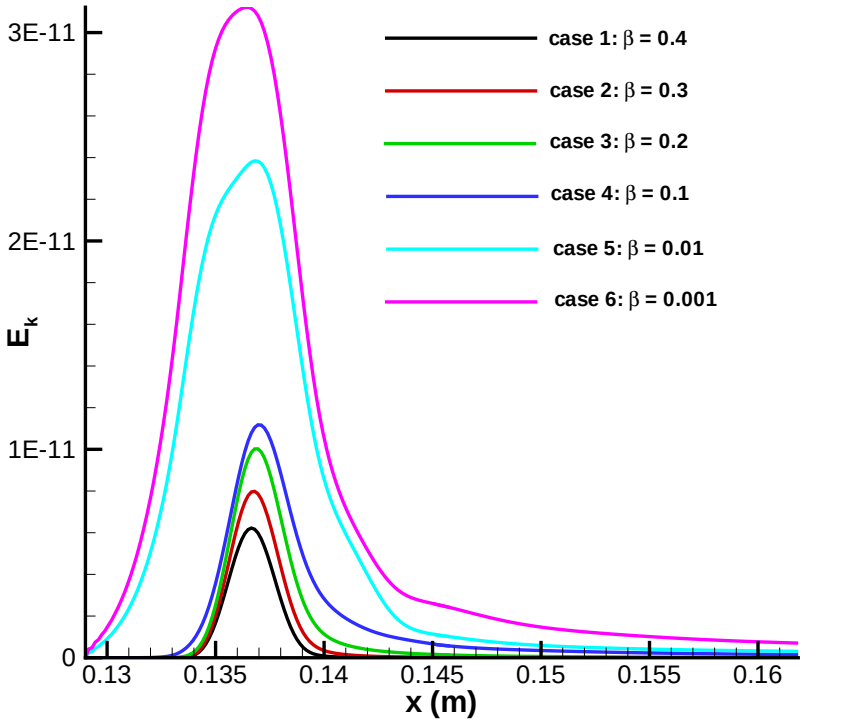

Figure 14: Comparison of the energy norm distribution along the flat plate near surface roughness in cases 1 to 6.

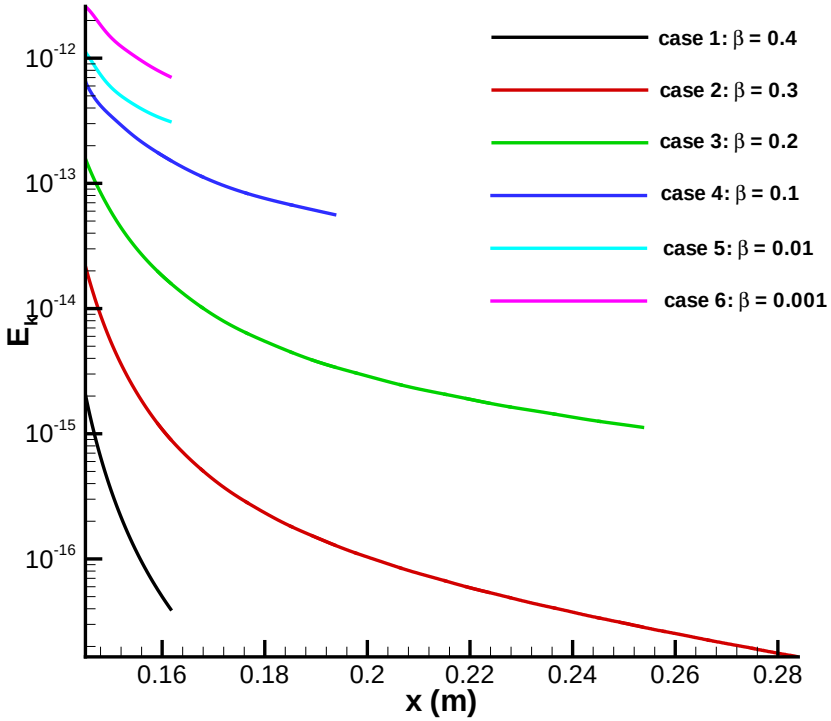

Figure 15: Comparison of the energy norm distribution along the flat plate downstream of surface roughness in cases 1 to 6.

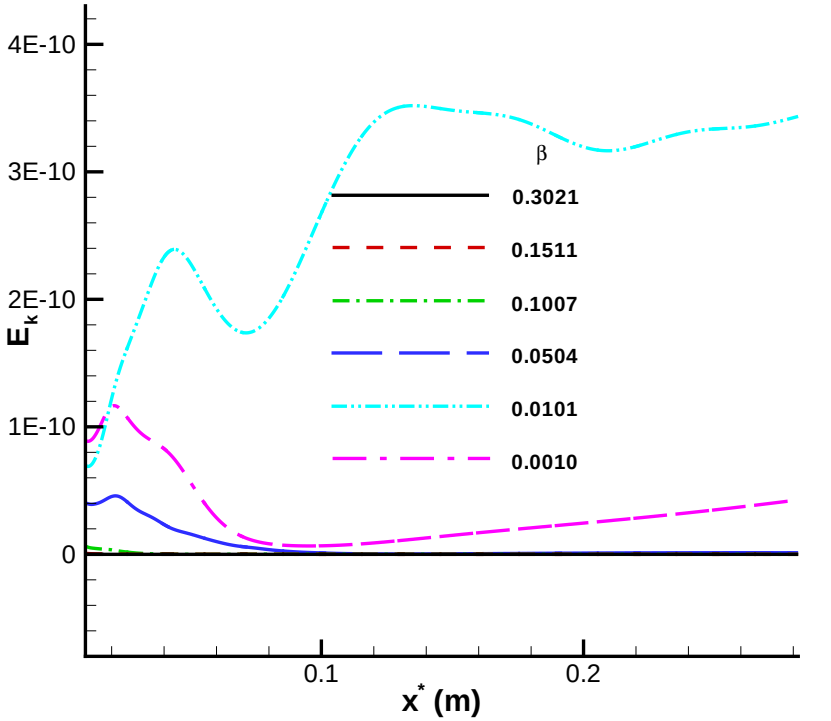

Figure 16: Energy norm distributions along the flat plate downstream of the roughness element [1].